RSC Advances

PAPER

View Article Online
View Journal | View Issue

Cite this: *RSC Adv.*, 2018, **8**, 2751

Hierarchical ZSM-5 nanocrystal aggregates: seed-induced green synthesis and its application in alkylation of phenol with *tert*-butanol†

Li Chen, Teng Xue, Haihong Wu * and Peng Wu

Received 27th November 2017
Accepted 5th January 2018

DOI: 10.1039/c7ra12811h

rsc.li/rsc-advances

Hierarchical ZSM-5 zeolite aggregates were synthesized in an organic-template-free system *via* seed-induced crystallization. The obtained samples were characterized using X-ray diffraction (XRD), scanning electron microscopy (SEM), transmission electron microscopy (TEM), N_2 adsorption–desorption, NH_3 temperature-programmed desorption (NH_3-TPD) and inductively coupled plasma atomic emission spectrometry (ICP-AES). The prepared ZSM-5 nanocrystalline aggregates possessed open/accessible hierarchical pores and active sites, showing significant advantages in the catalytic alkylation of phenol with *tert*-butanol. The obtained materials could maintain the activities of the nanocrystal zeolites and meanwhile could be easily separated or recovered during the preparation and reactions. This approach was simple and also overcame the commonly-seen drawbacks such as the exceeded use of specific templates or secondary templates during the synthesis of the hierarchical zeolites.

Introduction

Zeolites are microporous crystalline materials, widely used in catalysis as well as separation and purification fields due to their uniform small pore size, high internal surface area, flexible frameworks. They were mainly obtained in the form of micrometer-sized crystals before the development of colloidal zeolite synthesis in the early 1990s. Zeolite nanocrystals with crystal sizes smaller than 100 nm became a major event of the past decade in zeolite science.[1,2] Compared to conventional micrometer-sized zeolites, small zeolite crystals have short diffusion path lengths and thus reduced diffusion limitation, which is in favor of improving the catalytic efficiency. In addition, nano-sized zeolites possess large external surface areas and high surface activity, which become more important when the zeolites are intended to be used as catalysts in reactions involving bulky molecules.

Efforts have been made to the synthesis of nanocrystalline zeolites.[3] Generally, the synthesis of nano-sized zeolites are quite complex, which are deliberately controlled by organic template, silicon and aluminium sources, type of precursor in synthetic mixture and synthesis conditions.[3] A large amount of organic templates was usually desired to induce the fast nucleation and the formation of smaller crystals, and further to stabilize zeolite nanoparticles in the crystalline suspensions by the formation of a single organic layer on these nanoparticles, leading to enhanced repulsive forces between the zeolite nanocrystals.[4] However, the use of excessive amounts of expensive organic templates is not appreciated from the environmental and economical points of view. In addition, the organic templates required high temperature calcination of the zeolite to open the porosity, which leads to a volatile species which are far from being environmentally benign. At present, researchers have begun to pay attention reducing the dosage of templates. Nano-sized ZSM-5 zeolite was successfully synthesized in the absence of organic template after the aging for 24 h in the synthesis mixture, but no pure ZSM-5 zeolite could be obtained when the SiO_2/Al_2O_3 molar ratio reached 50.[4] An alternative approach that could address the requirements for environmentally benign and economically acceptable synthesis of nano-zeolites is the seed-crystallization. Colloidal zeolite seeds have already been proven to be effective in the nanocrystal zeolite production.[5,6] The quantity (or, more correctly, surface area) of added colloidal seeds had a great influence on the size of obtained final zeolites.[7] TPABr-silicalite-1 as structure directing agent was used to synthesize the MFI zeolite, but the obtained zeolites in size of 2–8 μm were still large crystal zeolite particles.[8] Majano *et al.* reported that zeolite ZSM-5 nanocrystals could be synthesized by seeding of an organic-template-free initial gel, but the crystal size of zeolites could be strongly affected by the crystallization temperature, crystals larger than 200 nm were obtained at 170 °C and much larger (400–700 nm) crystals were obtained at 170 °C when the synthesis time was extended to 24 h.[9] Reding *et al.* reported that the crystal size of final zeolite decreased from 300 nm to 100 nm with the amount of added silicalite-1 as seeds increased from 10 wt% to 33 wt%

Shanghai Key Laboratory of Green Chemistry and Chemical Processes, College of Chemistry and Molecular Engineering, East China Normal University, Shanghai 200062, P. R. China. E-mail: hhwu@chem.ecnu.edu.cn; Fax: +86 2162238510

† Electronic supplementary information (ESI) available. See DOI: 10.1039/c7ra12811h

of the total silica content.[10] However, large amount of TPAOH as template, TPAOH/SiO_2 = ~0.30, was still needed. Later, Xu *et al.* confirmed that the amount of added silicalite-1 seed could control the crystal size (100 nm to 6 μm) of ZSM-5 with less organic template (TPAOH/SiO_2 = 0.15).[11] Nevertheless, alternative methods of synthesis that would avoid the above mentioned drawbacks will be highly appreciated.

Furthermore, the recovery of nanoparticles should be also seriously considered from a practical application point of view, although discrete nanocrystalline zeolites were highly anticipated in some specific cases. One approach to solve the separation difficulties was to control the agglomeration and peptization of colloidal zeolites in aqueous media.[12] Considerable efforts had been devoted to dispersing zeolite nanocrystals in an inert matrix[13] or to shaping zeolite nanocrystals into macroporous aggregates.[14–16] However, it should be noted that most of the methods reported in literatures also resulted in an aggregate of nano-sized zeolites.[17] Therefore, it is possible to directly prepare the aggregate of nano-sized zeolites by finely tuning the synthetic parameters, where the aggregates in large size not only retain the properties of discrete nano-sized zeolite, but also can be easily separated or recovered during the preparation and reactions. Majano *et al.*[9] found that the level of crystal aggregation synthesized by seeding of an organic-template-free initial gel is much higher than the synthesis obtained from a clear solution rich in tetraalkylammonium hydroxides, where the high aggregation level was most probably due to the polycrystalline nature of colloidal seeds and possibly due to the presence of excessive sodium cations (Na_2O/SiO_2 = 0.296). Hierarchical ZSM-5 was also directly synthesized by controlling the nucleation, growth and template-free self-assembly of zeolite precursors formed in the initial stage of the zeolite crystallization process under the large amount of TPAOH (TPAOH/SiO_2 = 0.25) condition.[18] All these provided a useful background for the synthesis of nano-sized zeolites aggregates by finely tuning the synthetic parameters.

In this work, hierarchical ZSM-5 aggregates with nanocrystalline could be acquired using colloidal particles of TPAOH-silicalite-1 (denoted as 'seed' gel) in a common template-free alumina-silica gel system. This simple synthesis approach overcame the commonly-seen drawbacks in hierarchical zeolites synthesis where the exceeded amount of specific templates or secondary templates was used. The effect of SiO_2/Al_2O_3 ratio, H_2O/SiO_2 ratio and the amount of the 'seed' gel on the aggregate morphology of the ZSM-5 nanocrystals was investigated. The obtained hierarchical ZSM-5 zeolite aggregates exhibited large and irregularly-aggregated morphology with small primary zeolitic nanoparticles in size of about 50–80 nm with a narrow particle size distribution. Friedel–Crafts alkylation of phenol with *tert*-butanol as probe reaction was used to study the catalytic performance.

Results and discussion

The XRD of ZSM-5 zeolites aggregates with different molar compositions were shown in Fig. 1. The XRD patterns of HZ5-A prepared with the molar composition of

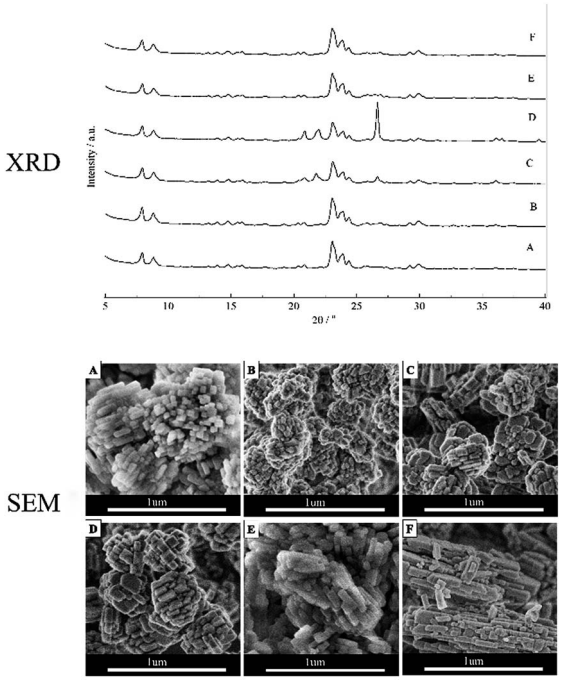

Fig. 1 XRD and SEM images of HZ5-A (A), HZ5-B (B), HZ5-C (C), HZ5-D (D), HZ5-E (E), HZ5-F (F).

$1SiO_2 : 0.033Al_2O_3 : 0.1Na_2O : 24H_2O$: seed (equal to 1.5 wt% of SiO_2) showed that the ZSM-5 zeolite aggregates were typical zeolite with MFI structure (Fig. 1A). When the $n(SiO_2)/n(Al_2O_3)$ molar ratio increased to 60 and 100, some impurities of α-quartz formed along with ZSM-5, which indicated that the aggregates ZSM-5 zeolite could be synthesized with a low $n(SiO_2)/n(Al_2O_3)$ ratio. And in case of variation of $n(H_2O)/n(SiO_2)$ and amount of seed gel, the high purity zeolite crystals could be obtained.

The morphologies of the ZSM-5 aggregates prepared with different synthesis ingredients were investigated and the SEM images were presented in Fig. 1. The hierarchical HZ5-A zeolite aggregates exhibited large and irregularly-aggregated morphology with size ranging from 0.6 to 0.8 μm and these aggregates were formed with small primary zeolitic nanoparticles in size of about 50–80 nm with a narrow particle size distribution (Fig. 1A). The small primary zeolitic nanoparticles in size of about 50–80 nm were smaller than the size of MFI zeolites reported,[8,9] when the seed was used to synthesize the MFI zeolite in the organic-template-free initial gel. The obtained hierarchical zeolite HZ5-B exhibited large and irregularly aggregated morphology in size of ~0.5 μm when the seed amount increased to 5 wt% with other synthesis ingredients unchanged. And these aggregates also consisted of small primary zeolitic nanoparticles in size of about 40–50 nm, as shown in the Fig. 1B, which could be attributed to the more seed appeared in the synthesis mixture and the smaller primary nanocrystal particles obtained. And the morphology, crystallinity and crystal size of the ZSM-5 aggregates were strongly affected by the $n(SiO_2)/n(Al_2O_3)$ ratio in the synthesis ingredients.[19] When the $n(SiO_2)/n(Al_2O_3)$ molar ratio changed from 30

to 60, the zeolites (denoted as HZ5-C) also exhibited large and irregularly aggregated morphology, while the primary zeolitic nanoparticle size of the HZ5-C (Fig. 1C) was slightly larger than that of HZ5-A under the same crystallization time. And when the $n(SiO_2)/n(Al_2O_3)$ molar ratio was further increased to 100 (denoted as HZ5-D), the primary zeolitic nanoparticle size of the HZ5-D was further increased, which were slightly larger than that of the HZ5-C (Fig. 1D). The size of zeolite aggregates (denoted as HZ5-E) became smaller in size of 0.3–0.4 μm and primary particles of the aggregates became closer at $n(H_2O)/n(SiO_2) = 13$, as shown in Fig. 1E. In the case of $n(H_2O)/n(SiO_2) = 50$ (denoted as HZ5-F), the primary nanoparticles of zeolite aggregates owned rod-like morphology with an obvious increment of *c*/*b* axis (Fig. 1F).

N_2 adsorption–desorption isotherms were shown in Fig. 2A, and the surface area, total pore volume and micropore volume of all the samples with different SiO_2/Al_2O_3 ratios are listed in Table 1. The isotherms are of type I & IV with hysteresis loops in the relative pressure range $P/P_0 = 0.5$–0.9, indicating the presence of irregular mesopores. The hysteresis loop could relate to some secondary porosity that is in contact with the exterior by channels of zeolite and is desorbing by cavitation. The BET surface of samples obtained at $n(SiO_2)/n(Al_2O_3)$ (molar ratio) = 30 were amounts to 310–370 $m^2\ g^{-1}$. They were in agreement with previously reported BET areas (nearly 300 $m^2\ g^{-1}$) on ZSM-5 zeolites,[20] indicating that the samples were highly crystalline MFI-type material. The BET surface area and micropore volume of the samples obtained when the $n(SiO_2)/n(Al_2O_3)$ molar ratio increased to 60 and 100 were a little below. This further suggested that the sample contained small amount of low surface area material (α-quartz) (Fig. 1). The HZ5-A presented the optimized textural properties with its relative large surface area (364 $m^2\ g^{-1}$ and pore volume 0.38 $cm^3\ g^{-1}$), indicating that this sample had been well crystallized and meanwhile retained the enriched mesopores within the nanocrystal aggregates.

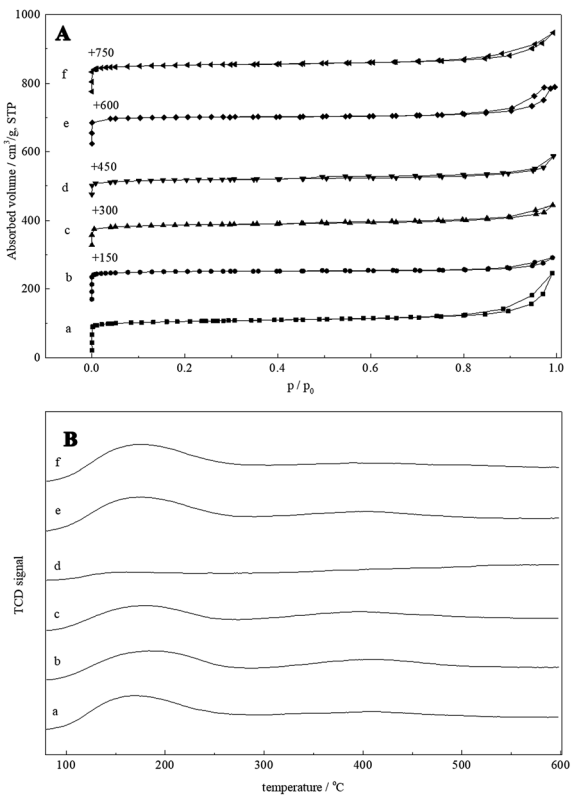

Fig. 2 (A) Nitrogen adsorption–desorption isotherms and (B) NH_3-TPD profiles of HZ5-A (a), HZ5-B (b), HZ5-C (c), HZ5-D (d), HZ5-E (e) and HZ5-F (f).

NH_3-TPD profiles of hierarchical ZSM-5 zeolite aggregate samples were shown in Fig. 2B and acidic properties were presented in Table 1. Here, all the as-synthesized samples had been directly ammonium ion exchanged to get the H-form ZSM-5 zeolites. All samples had similar-shaped curves and exhibited three resolved desorption peaks: the peak at *ca.* 110–250 °C attributed to desorption of NH_3 adsorbed on weak acidic sites, and the peak at *ca.* 250–400 °C attributed to desorption of NH_3 adsorbed on medium acidic sites, while the peak at *ca.* 300–550 °C assigned to strong acidic sites. The concentration of surface acid sites and the weak acid sites fraction of ZSM-5 synthesized at $n(SiO_2)/n(Al_2O_3)$ molar ratio 30 were similar, which were mainly attributed to the similar amount of accessible acid sites in these hierarchical zeolite aggregates. With the increasing of $n(SiO_2)/n(Al_2O_3)$ molar ratio, acid sites of the H-form ZSM-5 samples gradually decreased. From Table 1, the total acid sites of hierarchical ZSM-5 were little influenced although that the as-synthesized samples were directly ammonium ion exchange, which showed that it was not necessary to calcine the sample because as-synthesized ZSM-5 zeolite had open micropores. These features for the synthesis of ZSM-5 zeolite would be very important for avoiding environmental pollution and reducing production cost.

Acid catalyzed reactions such as Friedel–Crafts alkylation or acylation, rearrangement and *etc.* were important processes in organic synthesis, fine chemicals production as well as in petrochemical industry.[21,22] In recent years, solid acid catalysts such as zeolites or zeolite-like molecular sieves[23–25] have been replacing the conventional homogenous mineral acid catalysts.[22] However, the micropore size of zeolitic materials limits their applications as catalysts for bulkier molecules. Here, alkylation of phenol with *tert*-butanol (Friedel–Crafts alkylation) was used as a probe reaction to evaluate the catalytic performance of these hierarchical materials (Fig. 3). The phenol conversion was closely related to the acidity of the zeolite. The acid site density of hierarchical ZSM-5 kept almost invariable when the SiO_2/Al_2O_3 ratio was 30, and correspondingly the phenol conversion was similar. Phenol conversion gradually decreases with the increase of the silicon to aluminium ratio. Furthermore, the alkylation of phenol with *tert*-butanol took place in the micropores of zeolite ZSM-5 (0.54 × 0.56 nm), producing mainly the products smaller than the micropores of ZSM-5. To increase the selectivity of the bulky products, materials with large pore such as Al-MCM-41 could be used.[26] However, when Al-MCM-41 was used as catalyst for alkylation of phenol with *tert*-butanol, the conversion of phenol was usually lower due to the low acidity arising from the amorphous nature of Al-MCM-41. An effective way to increase the selectivity of the bulky products was to introduce hierarchical porosity to the

Table 1 Properties of hierarchical ZSM-5 zeolite aggregatesa

Samples	S_{BET} (m^2 g^{-1})	S_{ext} (m^2 g^{-1})	V_{total} (cm^3 g^{-1})	$V_{micropore}$ (cm^3 g^{-1})	Acidity (mmol NH_3 g^{-1})			$n(SiO_2)/n(Al_2O_3)$ in product
					Weak	Moderate	Strong	
HZ5-A	364	64	0.38	0.14	0.69	0.19	0.16	28.4
HZ5-B	359	42	0.26	0.14	0.57	0.18	0.13	29.2
HZ5-C	292	60	0.23	0.10	0.43	0.16	0.13	39.1
HZ5-D	226	47	0.18	0.08	0.11	0.03	0.02	65.7
HZ5-E	349	33	0.26	0.14	0.72	0.16	0.13	28.9
HZ5-F	360	41	0.28	0.14	0.71	0.15	0.12	28.2

tab1a S_{BET}: BET surface area calculated by BET method; V_{total}: total pore volume at $P/P_0 = 0.99$; $V_{micropore}$: micro-pore volume calculated by *t*-plot method.

microporous zeolite. The hierarchical ZSM-5 nanocrystal aggregates, with reduced primary crystal sizes and increased external surface area and mesopore volume, enhanced the chance for the reactions on the external surface, which was reflected by the increase of selectivity of bulky 2,4-DTBP (with the van der Waals radii of ~0.38 nm). HZ5-A possessed relatively large mesopore volume (0.24 cm^3 g^{-1}) and external surface (64 m^2 g^{-1}) and correspondingly exhibited high selectivity of bulkier molecules (2,4-DTBP) under the same reaction conditions. Moreover, the zeolite aggregates could be recovered by filtration conveniently during the reactions.

The reusability of heterogeneous catalysts was one of their main advantages. The fresh catalyst HZ5-A exhibited high phenol conversion of 31.4%. Correspondingly, reused catalysts of four time presented an activity of 30.6%, 30.1%, 29.3% and 29.5% respectively. These results indicated that the catalyst could be reused and almost maintained the initial activity even after four cycles. Such catalytic performance was of great importance for potential industrial application.

No ZSM-5 phase could be identified in the XRD pattern at the initial stage (0–1.5 h), indicating that the sample was still amorphous. With the crystallization time increased to 3.5 h, the weak characteristic diffraction peaks of MFI structure could be observed. When the crystallization time reached 5 h, the characteristic diffraction peaks of ZSM-5 zeolites were clearly observed and the broad peak at 20–30° belonging to the amorphous phase almost disappeared. The crystallinity of the products remained constant with the crystallization time after crystallizing for 8 h. This indicated that a much faster growth kinetics was observed compared with that of the reported zeolites synthesized by seed gels addition.[27] The nucleation and growth rate were greatly enhanced and the crystallization time was largely shortened due to the pre-added seed, as shown in Fig. 4B. Furthermore, obtained hierarchical ZSM-5 nanocrystal aggregates were stable and the crystallinity remained even after crystallizing for 168 h.

The morphology changes of alumina-silica during the crystallization process were characterized using SEM. As shown in Fig. 5, small particles in size of about 80–100 nm in the irregularly-shaped alumina-silica lumps could be observed at early stages of the hydrothermal reaction (0 min). The small particles might be the seeds added to the freshly precipitated alumina-silica (Fig. 5B). After 1.5 h, the small seed particles

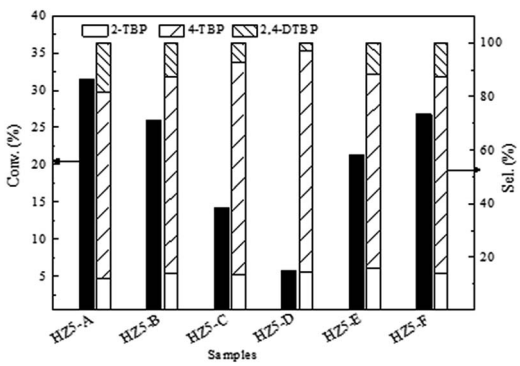

Fig. 3 Molar conversion of phenol and selectivity on HZ5-A, HZ5-B, HZ5-C, HZ5-D, HZ5-E and HZ5-F.

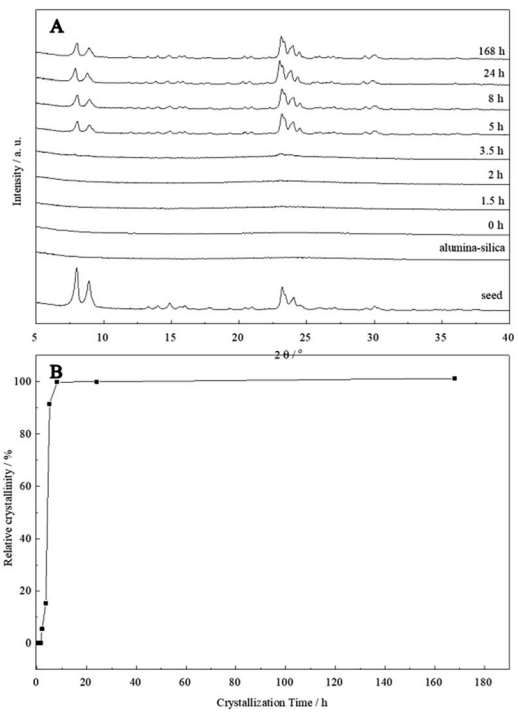

Fig. 4 XRD patterns of the HZ5-A samples crystallized at different time (A) and crystallization curve (B).

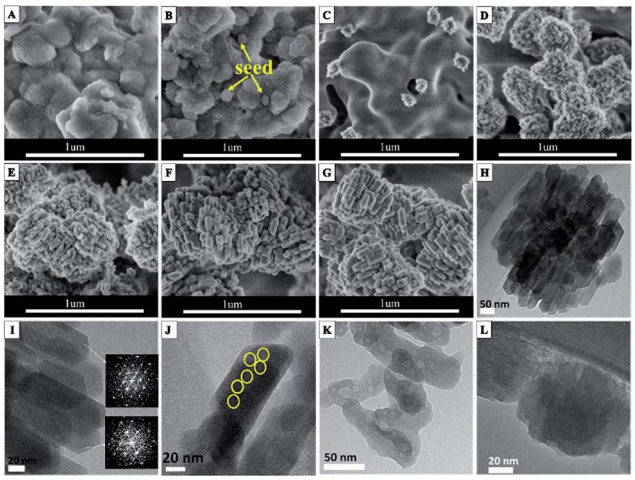

Fig. 5 SEM images of freshly precipitated alumina-silica (A) and as-synthesized HZ5-A crystallized for different time, 0 h (B); 1.5 h (C); 3.5 h (D); 5 h (E); 8 h (F); 24 h (G). TEM images of as-synthesized HZ5-A (H and I), as-synthesized HZ5-A treated by NaOH (0.2 M) solution for 0.5 h (J), HZ5-A treated by NaOH (0.4 M) solution for 4 h (K) and seed gel (L).

disappeared and some hedgehog-shaped aggregates encapsulated by 10 nm subnanocrystals randomly dispersed in the amorphous alumina-silica could be found, as shown in Fig. 5C. With the crystallization time increased to 3.5 h, more and more irregular hedgehog-shaped particles encapsulated by 10 nm subnanocrystals and alumina-silica transformed into aggregates with diameters of about 500 nm. It indicated that the seed might lead to the appearance of subnanocrystals which have the primary structure of MFI zeolites at first (Fig. 5D), then these subnanocrystals further induced the primary units [SiO_4] and [AlO_4] into a large amount of subnanocrystals, and the weak characteristic diffraction peaks of MFI structure were also detected by XRD (Fig. 4A 3.5 h). When the crystallization time reached 5 h, amorphous alumina-silica disappeared and only ZSM-5 aggregates were presented on the SEM (Fig. 5E). These aggregates were composed of primary zeolite nanoparticles in size of about 50–70 nm. The aggregates were stable and remained unchanged even after crystallizing for up to 168 h (Fig. 1A). The key scheme of hierarchical ZSM-5 zeolite aggregates formation could be illustrated in route of Scheme 1. In the typical synthesis, the small seed particles dissolved after adding to the freshly precipitated alumina-silica and some hedgehog-shaped aggregates encapsulated by 10 nm subnanocrystals dispersed in the amorphous alumina-silica could be found with

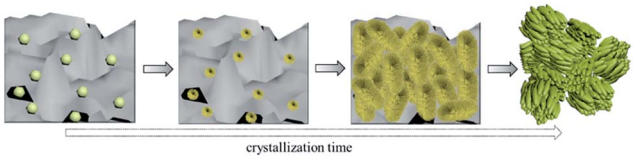

Scheme 1 Proposed formation process of hierarchically ZSM-5 zeolite aggregates using 'seed gels'.

increasing the crystallization time. And the hedgehog-shaped aggregates gradually grow up to about 500 nm with the further development of crystallization. Finally, the hierarchical ZSM-5 aggregates could be obtained. The crystalline nature of these units was evidenced by the diffraction fringes in the HRTEM image (Fig. 5I) and the corresponding selected area electron diffraction (Fig. 5I inset). Moreover, the presence of voids between the small primary units in TEM micrographs (Fig. 5H) suggested the existence of intercrystalline porosity in HZ5-A. The intercrystalline mesoporosity was further proved by an electron tomography (ET) study (Movie 1 in the ESI†). The mesopore channels were interconnected and accessible. This feature was of particular importance for the enhancement of the diffusion properties in the catalytic applications.[28]

In order to further reveal that distribution of silicon in the ZSM-5 nanocrystalline zeolite, alkaline desilication experiments were performed. The desilication of HZ5-A by varying NaOH concentration and time was performed. The resulting materials were characterized by HRTEM. When the HZ5-A was treated in 0.2 M NaOH for 0.5 h, the aggregate morphology turned to be dispersed nanoparticles along with relatively well-faceted crystallites and there are some irregular crystal defect in the nanocrystal (yellow area in Fig. 5J). Prolonging the treatment period, the well-faceted ZSM-5 crystallites disappeared and many irregular voids (in size of 5–10 nm) in the ZSM-5 zeolite crystals appeared (Fig. 5K). It is well known that these voids are formed due to the desilication in the interior zone which is rich of silica.[29] This result suggested that the external surface is rich of Al therefore remains unperturbed by the NaOH treatment.[29] With the NaOH concentration increasing up to 0.4 M, the hierarchical ZSM-5 aggregates were totally destructed and there were more irregular and larger voids in the ZSM-5 zeolite crystals as shown in Fig. 5K. The ICP-AES showed that SiO_2/Al_2O_3 ratio decreased from 28.4 to 7.1 after the desilication process. Notably the size and shape of voids were quite different from those of primary seed particles (Fig. 5L), which meant that the framework of HZ5-A was probably formed by a secondary nuclei process rather than growing along the outer-surfaces of the seed.[30] This assumption was consistent with our previous finding and other reports where the seed gels were dissolved and a secondary nuclei process occurred.[31]

Furthermore, ^{27}Al and ^{29}Si solid-state MAS NMR measurements were conducted to investigate the structural changes. As shown in Fig. 6A, only one peak at δ = 52.1–56.0 ppm corresponding to 4-coordinated Al species was observed for the samples crystallized for different periods. No 6-coordinated Al species, generally appearing at a chemical shift of ~0 ppm,[32] were observed throughout the synthesis, even in the mixture without heating (0 h). It was likely that all dissolved aluminate species reacted with silicates, due to their high affinity for bonding with silicates, and then became alumina-silica with 4-coordinated Al.[33] The chemical shift is sensitive to Al–O–Si bond angles. The peak shifted from 54.6 to 53.8 ppm 168 h of heating (see Fig. 6B, right axis). This indicates an increase in the average Al–O–Si angles. Full width at half-maximum (FWHM) of the 4-coordinated peaks was plotted in Fig. 6B (left axis). FWHM of the peaks decreased dramatically during the first 5 h of

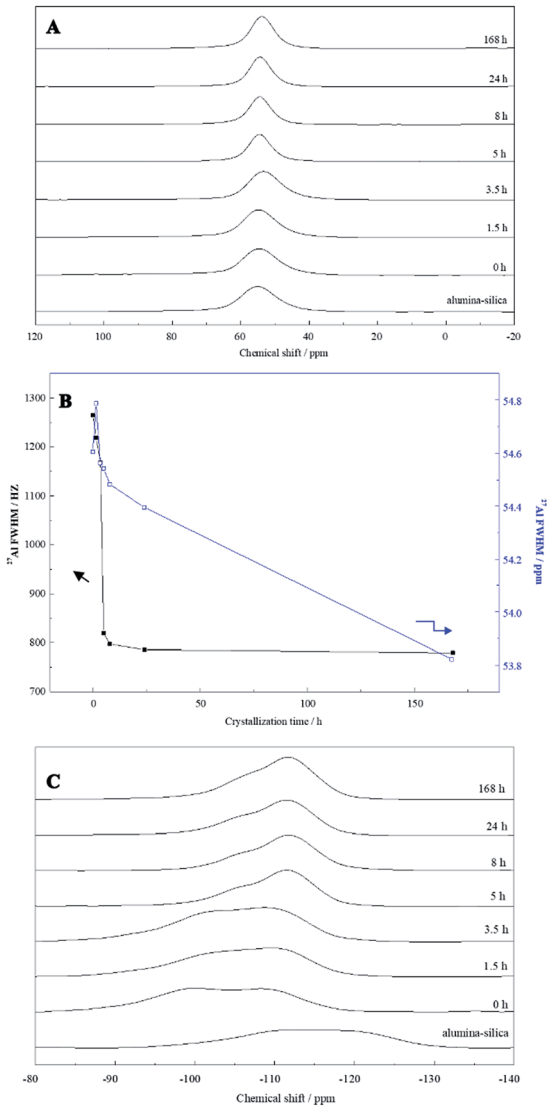

Fig. 6 (A) ^{27}Al MAS NMR spectra and (B) full width at half-maximum (left axis) and position (right axis) of each NMR peak of the products synthesized for different periods of time. And (C) ^{29}Si MAS NMR spectra of the products synthesized for different periods of time.

hydrothermal treatment, suggesting that the structure of alumina-silica become more ordered, that is, narrower distributions of Al–O–Si angles. Combined with the XRD and SEM results described above, it was postulated that the dissolved aluminate species seemed to react with silicate species, resulting in aluminosilicate species and then the crystalline structure of MFI. FWHM decreased slowly during further heating for up to 3.5 h, suggesting that the structural order of amorphous alumina-silica was gradually enhanced during this induction period. Upon heating between 5 h and 168 h, the observed down-field shift of NMR peak from 54.6 to 53.8 ppm (see Fig. 6B, right axis) indicates a decrease in the average Al–O–Si angles. With the formation of ZSM-5 zeolite (5–168 h), FWHM decreased rapidly (see Fig. 6B, left axis), evidencing the well-ordered zeolite ZSM-5 crystals obtained. Fig. 6C showed ^{29}Si MAS NMR spectra. The aluminosilicate was rich in Q^4(0Al) silicon species ($Si(SiO)_4$) as the spectrum showed the strongest signal around $\delta = -110$ ppm.[27] However, the ^{29}Si MAS NMR spectra of alumina-silica added seed gel (0 h) indicated a main peak at a chemical shift of *ca.* −110 ppm for Q^4 species with a shoulder centered at −100 ppm, assigned to Q^3(0Al) ($(SiO)_3$-SiOH or $(SiO)_3SiO^-$) or Q^4(2Al) ($Si(AlO)_2(SiO)_2$) silicon species. With increasing hydrothermal treatment time, the signal intensities had gradually raised at about −110 ppm indicated the increase in Q^4(0Al) species. Further hydrothermal treatment up to 8 h resulted in the appearance of a sharp, outstanding peak at −110 ppm together with a shoulder at higher chemical shifts, indicating the enhanced structural order and condensation of silicates with the formation of ZSM-5 zeolite. Thus it could be seen that the structural change of alumina-silica in the crystallization process fully were consistent with the result of SEM and XRD, the resulting ZSM-5 aggregates materials could be synthesized by the seed with a secondary nuclei crystallization.

Conclusions

In summary, ZSM-5 zeolite aggregates with open and accessible hierarchical pores were synthesized by seed-assistant method, where no secondary template and additives were added. The seed played a key role in assembling hierarchical ZSM-5 aggregates through dissolution into subnanocrystals with MFI primary structure and inducement of the $[SiO_4]$ and $[AlO_4]$ primary units into a large amount of subnanocrystals simultaneously. This method showed several advantages in zeolite synthesis: circumventing the use of abundant organic templates/secondary templates and consequent calcination step; and hierarchical zeolite aggregates with larger BET surface area (S_{BET}) and meso-volume showing high catalytic performance in Friedel–Crafts alkylation. This approach addresses the requirements for environmentally-friendly and economically affordable synthesis of nano-zeolite or aggregates.

Experimental

Materials synthesis

The 'seed' gel was prepared according to previous report.[34] In a typical process, a homogeneous clear solution of tetrapropylammonium hydroxide (TPAOH) and tetraethyl orthosilicate (TEOS) with molar ratio of TPAOH : TEOS = 0.35 : 1 was heated to 80 °C for the evaporation of a desired amount of ethanol. Then the water required was added to obtain a mixture with molar composition of $1SiO_2 : 0.35TPAOH : 20H_2O$. Finally the resulting mixture was transferred into Teflon-lined stainless autoclave and heated under autogenous pressure at 100 °C for 24 h. After cooling to room temperature, the mixture (denoted as 'seed') was directly used.

The hierarchical ZSM-5 zeolite aggregates were synthesized as follows: a solution of $Al_2(SO_4)_3 \cdot 18H_2O$ dissolved in an aqueous HCl solution was added dropwise to an aqueous solution of $Na_2SiO_3 \cdot 9H_2O$. The freshly precipitated alumina-silica was obtained by filtration after being continuously stirred for 2 h. Subsequently, the obtained solid was added to H_2O

Table 2 Compositions of the hierarchical ZSM-5 zeolite aggregates

	Composition in molar ratios				
Samples	SiO_2	Al_2O_3	Na_2O	H_2O	Seed[a]
HZ5-A	1	0.033	0.1	24	0.015
HZ5-B	1	0.033	0.1	24	0.05
HZ5-C	1	0.067	0.1	24	0.015
HZ5-D	1	0.010	0.1	24	0.015
HZ5-E	1	0.033	0.1	13	0.015
HZ5-F	1	0.033	0.1	50	0.015

[a] Based on the total SiO_2.

and the required seed gel. The molar composition of the synthetic mixtures was $1SiO_2 : 1/x\ Al_2O_3 : 0.1Na_2O : yH_2O$: seed gel, (equal to z wt% of SiO_2; $x = 30, 60, 100$; $y = 13, 24, 50$; $z = 1.5, 5$, respectively). After being stirred for 2 h, the mixtures were transferred into a Teflon-lined stainless steel autoclave, where they were heated at 175 °C statically under autogenous pressure for the prescribed time (0–168 h). The obtained products were filtered, washed and then dried overnight at 100 °C. To get the H-form ZSM-5 zeolites, the as-synthesized samples were directly ion-exchanged using 0.6 M NH_4NO_3 solution at 80 °C for 2 h without calcination and then calcined at 550 °C in air for 6 h. The obtained samples were denoted as HZ5-X (X = A, B, C, D, E, F) based on the molar compositions as shown in Table 1. Here, without a subsequent calcination, all the as-synthesized samples had been directly ammonium ion exchange and the H-form ZSM-5 zeolites were obtained by ion exchange (4 times) with 0.6 M NH_4NO_3 solution at 80 °C for 1 h, follow by calcination at 550 °C in air for 6 h (Table 2).

Characterization and catalytic test

The particle sizes and morphology of the hierarchical zeolite aggregates were characterized by scanning electron microscopy (type HITACHI S-4800) with an accelerating voltage of 3 kV. Transmission electron microscopy (TEM) characterization was carried on a FEI TECNAI G^2 F30 operated at 300 KV. For the TEM images, the specimens were dispersed in ethanol and placed on holey copper grids. The X-ray diffraction (XRD) patterns were collected on a Rigaku Ultima IV diffractometer with Cu-Kα radiation ($\lambda = 1.5405$ Å) at 35 kV and 25 mA in the 2θ angle range of 5–40°. The surface area, pore volume, and pore size distribution of the different materials was measured from N_2 adsorption/desorption isotherms at −196 °C on a BELSORP-MAX instrument. Prior to the measurements, the samples were degassed at 300 °C under vacuum for at least 4 h. The surface areas were calculated by the Brunauer–Emmett–Teller (BET) method using the data in the relative pressure range of $0.05 < p/p_0 < 0.25$. The total pore volumes were measured at $p/p_0 = 0.99$, and the micropore volume was calculated from the t-plot method. The acidity was measured by ammonia temperature-programmed desorption (NH_3-TPD) using TP-5080 chemisorption instrument (Xianquan Co., Ltd, Tianjin, China). 100 mg of the H-type samples were pretreated at 600 °C for 2 h under helium flow and NH_3 adsorption was carried out at 80 °C. The temperature was then raised to 600 °C at a rate of 10 °C min^{-1} and the TPD profiles for chemisorbed NH_3 were monitored by a TCD detector. Inductively coupled plasma atomic emission spectrometry (ICP-AES) was obtained on a Thermo IRIS Intrepid II XSP atomic emission spectrometer after dissolving the samples in HF solution. ^{27}Al and ^{29}Si solid-state MAS NMR spectra were recorded on a Bruker DSX300 spectrometer.

The alkylation of phenol with *tert*-butanol was carried out at 125 °C for 4 h under stirring in a 50 ml round-bottomed flask immersed in a thermostatic oil bath and equipped with a condenser. The stirring was sufficiently strong to rule out the external diffusion on catalytic performance for all of the batches. In a typical batch, 0.15 g of catalyst, 7.78 g of cyclohexane as solvent, 0.74 g of *tert*-butanol and 0.47 g of phenol were used. The product was analyzed using a Shimadzu GC-2014 gas chromatograph equipped with a 30 m Wax capillary column and a flame ionization detector.

Conflicts of interest

There are no conflicts to declare.

Acknowledgements

We gratefully acknowledge the financial support by NSFC (21503081 and 21573073), China Ministry of Science and Technology (2016YFA0202800) and Shanghai Leading Academic Discipline Project (No. B409).

References

1 J. P. Verduijn, Patent No. WO 93/08125, 1993.
2 C. Y. Hsu, A. S. T. Chiang, R. Selvin and R. W. Thompson, *J. Phys. Chem. B*, 2005, **109**, 18804–18814.
3 L. Tosheva and V. P. Valtchev, *Chem. Mater.*, 2005, **17**, 2494–2513.
4 S. Mintova, J. Gilson and V. Valtchev, *Nanoscale*, 2013, **5**, 6693–6703.
5 J. P. Verduijn, M. M. Mertens, W. J. Mortier, M. J. G. Janssen, C. W. M. van Oorschot and D. E. W. Vaughan, Patent No. WO 006492, 2000.
6 J. P. Verduijn, Europe pat. No. 0753483, 1997.
7 C. S. Cundy and P. A. Cox, *Microporous Mesoporous Mater.*, 2005, **82**, 1–78.
8 M. Razavian, S. Fatemi and M. Komasi, *Mater. Res. Bull.*, 2015, **65**, 253–259.
9 G. Majano, A. Darwiche, S. Mintova and V. Valtchev, *Ind. Eng. Chem. Res.*, 2009, **48**, 7084–7091.
10 G. Reding, T. Mäurer and B. Kraushaar-Czarnetzki, *Microporous Mesoporous Mater.*, 2003, **57**, 83–92.
11 F. Xu, M. Dong, W. Y. Gou, J. F. Li, Z. F. Qin, J. G. Wang and W. B. Fan, *Microporous Mesoporous Mater.*, 2012, **163**, 192–200.
12 T. Mäurer, S. P. Müller and B. Kraushaar-Czarnetzki, *Ind. Eng. Chem. Res.*, 2001, **40**, 2573–2579.

13 C. Madsen and C. J. H. Jacobsen, *Chem. Commun.*, 1999, 673–674.
14 B. T. Holland, L. Abrams and A. Stein, *J. Am. Chem. Soc.*, 1999, **121**, 4308–4309.
15 L. M. Huang, Z. B. Wang, J. Y. Sun, L. Miao, Q. Z. Li, Y. S. Yan and D. Y. Zhao, *J. Am. Chem. Soc.*, 2000, **122**, 3530–3531.
16 B. Zhang, S. A. Davis and S. Mann, *Chem. Mater.*, 2002, **14**, 1369–1375.
17 R. Selvin and A. S. T. Chiang, *J. Nanosci. Nanotechnol.*, 2014, **14**, 7351–7359.
18 Z. P. Wang, C. Li, H. J. Cho, S.-C. Kung, M. A. Snyderc and W. Fan, *J. Mater. Chem. A*, 2015, **3**, 1298–1305.
19 C. S. Cundy, B. M. Lowe and D. M. Sinclair, *Faraday Discuss.*, 1993, **95**, 235–252.
20 S. Sang, F. Chang, Z. Liu, C. He, Y. He and L. Xu, *Catal. Today*, 2004, **93–95**, 729–734.
21 G. A. Olah, *Friedel–Crafts and Related Reactions*, Interscience, New York, 1964, vol. 2–3.
22 P. B. Venuto and P. S. Landis, *Adv. Catal.*, 1968, **18**, 259–371.
23 W. Holderich, M. Hesse and F. Naumann, *Angew. Chem., Int. Ed. Engl.*, 1988, **27**, 226–246.
24 C. B. Dartt and M. E. Davis, *Catal. Today*, 1994, **19**, 151–186.
25 J. H. Clark and D. J. Macquarrie, *Org. Process Res. Dev.*, 1997, **1**, 149–162.
26 S. K. Badamali, A. Sakthivel and P. Selvam, *Catal. Today*, 2000, **63**, 291–295.
27 T. Xue, L. Chen, Y. M. Wang and M.-Y. He, *Micropor. Mesopor. Mater.*, 2012, **156**, 97–105.
28 R. van Grieken, J. L. Sotelo, J. M. Menendez and J. A. Melero, *Microporous Mesoporous Mater.*, 2000, **39**, 135–147.
29 J. C. Groen, T. Bach, U. Ziese, A. M. Paulaime-van Donk, K. P. de Jong, J. A. Moulijn and J. Pérez-Ramírez, *J. Am. Chem. Soc.*, 2005, **127**, 10792–10793.
30 N. Ren, Z. J. Yang, X. C. Lv, J. Shi, Y. H. Zhang and Y. Tang, *Microporous Mesoporous Mater.*, 2010, **131**, 103–114.
31 D. Wang, X. Li, Z. Liu, Y. Zhang, Z. Xie and Y. Tang, *J. Colloid Interface Sci.*, 2010, **350**, 290–294.
32 G. Engelhardt and D. Michel, *High-Resolution Solid-State NMR of Silicates and Zeolites*, John Wiley & Sons, New York, 1987.
33 T. Ikuno, W. Chaikittisilp, Z. D. Liu, T. Iida, Y. Yanaba, T. Yoshikawa, S. Kohara, T. Wakihara and T. Okubo, *J. Am. Chem. Soc.*, 2015, **137**, 14533–14544.
34 B. J. Schoeman, *Microporous Mesoporous Mater.*, 1998, **22**, 9–22.

